Imaging Tumor Vascular Heterogeneity and Angiogenesis using Dynamic Contrast-Enhanced Magnetic Resonance Imaging

Alan Jackson,[1] James P.B. O'Connor,[1,2] Geoff J.M. Parker,[1] and Gordon C. Jayson[2]

Abstract   This article reviews the application of dynamic contrast-enhanced magnetic resonance imaging in both clinical studies and early-phase trials of angiogenesis inhibitors. Emphasis is placed on how variation in image acquisition and analysis affects the meaning and use of derived variables. We then review the potential for future developments, with particular reference to the application of dynamic contrast-enhanced magnetic resonance imaging to evaluate the heterogeneity of tumor tissues.

Development of quantitative biomarkers has led to increased use of imaging in the evaluation of tumor angiogenesis (1, 2). Magnetic resonance imaging (MRI) has been the most commonly used modality due to its wide availability and lack of ionizing radiation—two features that provide significant benefits over positron emission tomography. Also, although MRI does not offer the high level of biological specificity available with positron emission tomography ligands, it does provide a wide range of physiologically relevant image contrasts that make it a flexible imaging modality.

In dynamic contrast-enhanced MRI (DCE-MRI), the distribution of i.v. administered contrast agent is repeatedly imaged. Subsequent analyses produce biomarkers of the tumor vasculature. The technique is of interest to clinical oncologists for two main reasons. First, DCE-MRI biomarkers of drug efficacy and clinical outcome are used in an increasing number of early-phase clinical trials of antiangiogenic and vascular disrupting agents. Second, the technique has been applied in the nontrial setting to differentiate benign pathology from malignant disease, to grade tumors noninvasively, to detect early relapse, and to predict clinical outcome after both cytotoxic chemotherapy and radiation therapy (3).

DCE-MRI data analysis is complex. The variables obtained are heavily dependent on the choice of acquisition strategy (e.g., single slice, multislice, or three-dimensional imaging) and image analysis method [e.g., definition of the region of interest (ROI), selection of an arterial input function (AIF), and choice of pharmacokinetic model]. Crucially, all these factors can influence not only the value but also the precise meaning of derived variables. Furthermore, acquisition and analysis methods vary considerably between studies (4–6). These technical issues are considered in Appendix 1. In the remainder of this article, we begin by reviewing the application of DCE-MRI in clinical studies and in trials of angiogenesis inhibitors. We then discuss the application of DCE-MRI to investigate tumor heterogeneity because this illustrates an important potential use of functional imaging techniques in the evaluation of anticancer therapy.

Applications of DCE-MRI

Clinical adoption of DCE-MRI has been slow. Many studies have used simplified measurements of change in signal intensity for their analyses. Such metrics characterize the shape of the signal-time course curve or describe the rate of increase in signal intensity (7, 8), but show poor reproducibility and do not distinguish the effects of blood flow, blood volume, and contrast agent leakage (9). The application of T_1-weighted DCE-MRI to early-phase clinical trials of angiogenesis inhibitors has driven developments in quantitative image analysis, particularly the modeling of variables that describe tumor microvascular structure and function (Fig. 1). The details of these alternative analysis techniques are discussed in Appendix 1.

Clinical Applications of DCE-MRI

Analysis of enhancement kinetics (commonly from very low temporal resolution acquisitions) has become standard for the diagnostic classification of lesions in the breast and the liver. In the breast, it is common to calculate enhancement rates from regions of interest placed within suspicious lesions (10) with simple signal intensity metrics such as the proportion of maximal enhancement that occurs over a given time (e.g., 80%/min; ref. 8). Although malignant lesions tend to have higher enhancement rates, no fixed threshold provides a reliable distinction. Evidence of early washout of contrast agent has also been strongly associated with malignancy (11). Furthermore, enhancement patterns help identify histologic

Authors' Affiliations: [1]Imaging Science and Biomedical Engineering, University of Manchester and [2]Cancer Research UK, Department of Medical Oncology, Christie Hospital, Manchester, United Kingdom

Requests for reprints: James P.B. O'Connor, Imaging Science and Biomedical Engineering, University of Manchester, Ground Floor, Stopford Building, Oxford Road, Manchester M13 9PT, United Kingdom. Phone: 44-161-275-5770; Fax: 44-161-275-1138; E-mail: james.o'connor@manchester.ac.uk.
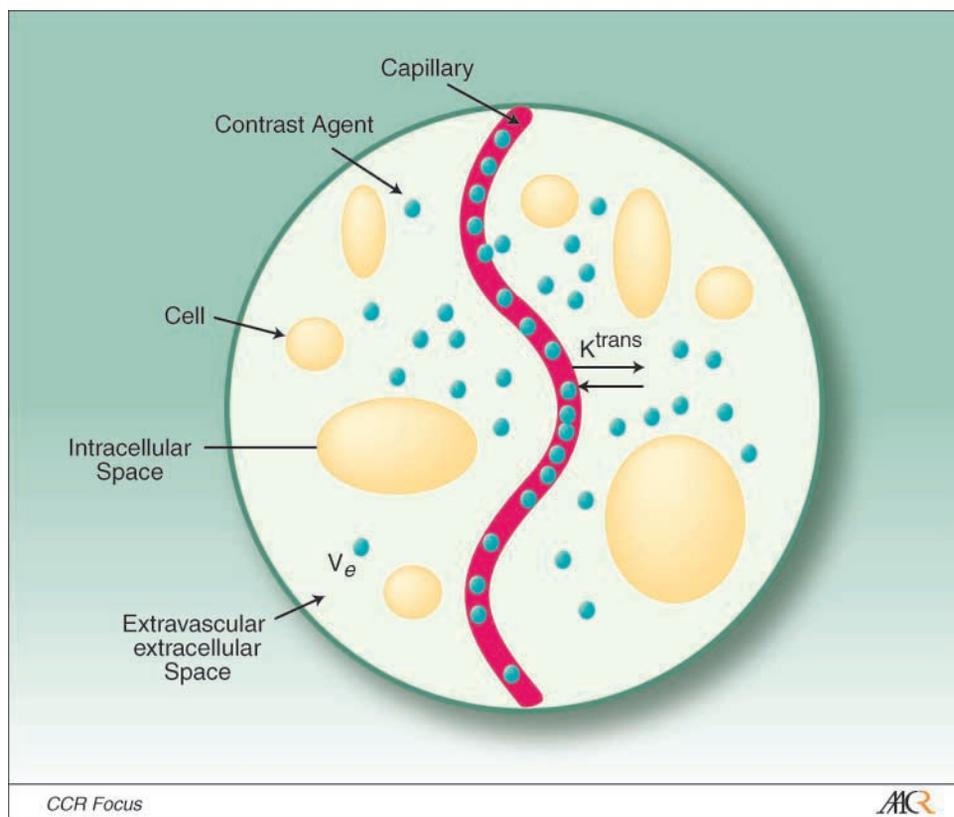
Fig. 1. Compartmental modeling of the tumor microvasculature in a single MRI voxel. Contrast molecules (*green dots*) enter the tissue through a blood vessel, approximated by the AIF. Some contrast agent remains in the vessel, enabling calculation of plasma volume (v_p) within the tissue and some leaks into the extracellular space. Clinically available MRI contrast agents do not leak into the intracellular space. The volume transfer constant of contrast agent (K^{trans}) leakage is determined by the contrast concentration difference between the intravascular and extravascular space, flow (F), and the product of the capillary surface area (S) and permeability (P). MRI signal change will also be affected by the proportional size of the extravascular extracellular space (v_e).

subtypes and predict response to radiotherapy and overall prognosis (12–14). Characterization of liver lesions is improved by examination of the enhancement rate and pattern (i.e., the spatial heterogeneity) and by examination of changes in enhancement on late scans (15).

In the brain, T_2*-weighted imaging of glioblastoma multiforme has repeatedly shown heterogeneity in cerebral blood volume (CBV) parametric maps (Fig. 2), where areas of high CBV correlate to regions of high-grade malignancy (16–18). Consequently, the practice of targeting biopsy to an area of high CBV has been adopted in many specialist centers (19). In addition, measurement of volume transfer coefficient of contrast agent across the capillary wall (K^{trans}) has been shown to independently predict prognosis using T_1-weighted sequences, further supporting use of DCE-MRI in the management of brain tumors (18, 20).

There is also increasing evidence that DCE-MRI may have further oncological applications. Characterization of prostate carcinoma lesions and their discrimination from benign disease can be improved by using dynamic contrast-enhanced analysis (21). Other potential applications include monitoring the response of osteosarcoma to chemotherapy (22), evaluation of the effect of radiotherapy early in treatment in cervical carcinoma (23), and using DCE-MRI to predict event-free survival in multiple myeloma (24). In general, as simple analysis packages, often using signal intensity metrics, become commercially available, indications for using dynamic contrast-enhanced computed tomography and MRI in follow-up and treatment evaluation are increasing (1, 25, 26).

DCE-MRI in Clinical Trials of Angiogenesis Inhibitors

Approximately 30 DCE-MRI–based studies of antiangiogenic (27–50) and vascular targeting agents (51–56) have been reported to date, predominantly in phase I trials, although a few phase II studies have incorporated the technique. Image acquisition, analysis, and principal findings have been extensively reviewed elsewhere (57). Nearly all of these studies have utilized T_1-weighted DCE-MRI. Some studies have also incorporated positron emission tomography, T_2*-weighted DEC-MRI, and/or other functional imaging techniques.

Modeled DCE-MRI variables are subject to random error, biological variation and measurement inaccuracies. All of these factors cause day-to-day variation in measured values; thus, it is necessary to calculate confidence intervals for each combination of DCE-MRI model, choice of AIF, and variable. Some consensus has been reached on what degree of change is likely to represent true change—for example, most studies accept a change in K^{trans} of >40% as likely to represent a true difference due to drug effect—but in practice the precise confidence interval varies between studies depending on image acquisition and analysis variables (58, 59). For this reason, many centers have routinely done two baseline examinations to calculate variable reproducibility for an individual phase I trial (32, 44, 53).

Some trials have reported model-free analyses based on the initial area under the gadolinium contrast agent concentration-time curve (IAUGC), but the majority have used some form of

pharmacokinetic analysis either alone or in combination with IAUGC (57). When modeling has been applied, most have adopted a simple model with only a minority attempting to correct for intravascular contrast effects. Despite this, evidence for drug efficacy has been found in several compounds, including the anti–vascular endothelial growth factor antibody bevacizumab (Avastin; Genentech; ref. 49); the tyrosine kinase inhibitors vatalanib (PTK787/ZK222584; Novartis; refs. 29, 36, 37, 47, 60), axitinib (AG-013736; Pfizer; ref. 34), BIBF1120 (Boehringer Ingelheim; ref. 39), and cediranib (AZD2171; AstraZeneca; ref. 30); and the antitubulin agent combretastatin A4-phosphate (CA-4-P; OxiGene; ref. 53). In each of these trials, significant reduction in IAUGC, K^{trans}, or K_i (the unidirectional transfer constant, a similar variable to K^{trans}) was observed after treatment. Finally, in some cases, the effective or biologically active dose was, in part, defined by the DCE-MRI biomarker (30, 46, 53).

Despite these encouraging results, identification of change in the tumor microvasculature does not necessarily predict success at phase III evaluation (61). Few trials of angiogenesis inhibitors have described a clear correlation in DCE-MRI biomarker with progression-free survival, the notable exception being sorafenib (BAY43-9006; Bayer; ref. 42). Details of image acquisition, analysis, and findings in some of the key trials are presented in Table 1, which highlights the considerable variation in choice of image acquisition and analysis.

Limitations of DCE-MRI Biomarkers in Oncology

No DCE-MRI variable has yet been accepted as a validated surrogate end point for use in phase III trials or routine clinical practice. Several points must be considered here. First, variables represent composites of physiologic processes rather than absolute measurements of flow or capillary permeability. Hence, a variable such as K^{trans} will not accurately measure flow or permeability—indeed, its precise meaning will vary between examinations. Second, there is evidence that the pharmacokinetic models used in DCE-MRI systematically overestimate K^{trans} and underestimate the blood plasma volume fraction (v_p; ref. 62). Third, considerable variations in measurement reproducibility reduce the confidence limits for individual measurements in a clinical setting.

Fourth, validation of DCE-MRI variables against histologic and serum biomarkers of angiogenesis is incomplete. Broad correlations between various MRI variables have been shown with tumor microvascular density (63); however, the marked variation in image acquisition and analysis between studies make comparison difficult. For example, several studies have correlated signal intensity metrics with microvascular density in patients with breast cancer. Amplitude and time to enhancement have been shown to correlate with microvascular density (64, 65); however, this has not been widely replicated (66). Furthermore, a linear relationship between the MRI efflux rate constant (k_{21}), which approximates to a measure of vascular permeability and surface area, has been reported with tissue vascular endothelial growth factor staining, although no relationship was found with microvascular density (10). This, in part, reflects the problem of comparing MRI changes measured at the millimeter level with either histology markers of vessel structure or distribution of receptors at the micrometer scale, or with circulating levels of angiogenic growth factors. Furthermore, microvascular density is a measurement of vessel density, whereas MRI variables such as v_p reflect the average density and are sensitive only to perfused vessels.

Finally, only a small number of DCE-MRI clinical studies have shown evidence for predicting clinical outcome. Examples include signal intensity metrics predicting local recurrence (67) and survival (68) in patients with cervical carcinoma and K^{trans} as an independent prognostic indicator of survival in patients with high-grade glioma (20). Lack of comprehensive validation against clinical outcome data currently prevents the use of DCE-MRI biomarkers as an accepted surrogate end point in a phase III trials or in clinical studies.

Fig. 2. T_1-weighted anatomic image in a patient with a glioblastoma multiforme in the right cerebral hemisphere (*left*) with a parametric map of CBV calculated from T_2^*-weighted dynamic MRI data (*right*; no units).
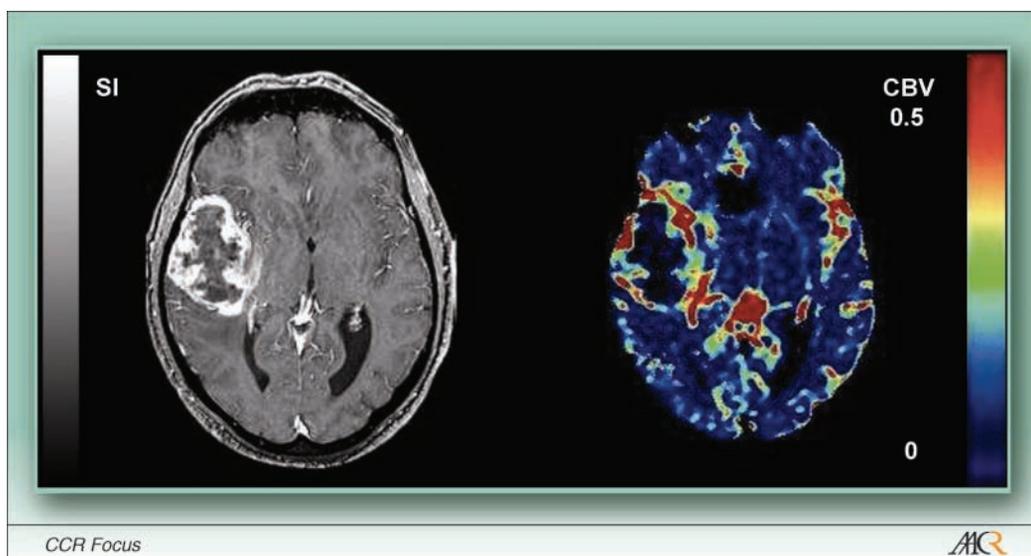
Table 1. Selected trials of angiogenesis inhibitors evaluated by DCE-MRI

Tumor group*	Agent	n	Acquisition	AIF [†]	DCE-MRI biomarker [‡]	ROI [§]	Principal findings	Reference
Anti-VEGF antibody								
Mixed	HuMV833	20	Three-dimensional	Measured	K^{trans}, k_{ep}, v_p	Pixel based	Reduction in k_{ep} but no dose relationship	Jayson et al. (33)
Breast	Bevacizumab	20	—	Measured	K^{trans}, v_e	Whole tumor	Reduction in K^{trans} of 34%	Wedam et al. (49)
Tyrosine kinase inhibitor								
GBM	PTK/ZK	14	T_1- and T_2*-weighted	—	K_i, CBV	—	Dose-dependent reduction in K_i predicts progression	Conrad et al. (29)
CRC	PTK/ZK	26	Two-dimensional single slice	Assumed (FH)	K_i	Whole tumor	Dose-dependent reduction in K_i predicts RR and progression	Morgan et al. (36)
Mixed	PTK/ZK	27	Two-dimensional single slice	Assumed (FH)	K_i	Whole tumor	Dose-dependent reduction in K_i predicts RR and progression	Mross et al. (37)
Mixed	AZD2171	24	Two-dimensional single slice	—	IAUGC	Whole tumor	Reduction in IAUC of ≥40% defined dose	Drevs et al. (30)
GBM[‖]	AZD2171	16	Three-dimensional and T_2*-weighted	—	K^{trans}, v_e, CBV, CBF	Pixel based	Reduction in K^{trans} and v_e	Batchelor et al. (28)
Mixed	AG-013736	17	Three-dimensional	Measured	IAUGC, K^{trans}	Whole tumor	Dose-dependent reduction in IAUGC and K^{trans}	Liu et al. (34)
RCC	BAY43-9006	12	—	—	K^{trans}, v_e	—	Reduction in K^{trans} predicts RR and PFS	O'Dwyer et al. (42)
Mixed	BIBF1120	35	Two-dimensional multislice	Assumed (FH)	IAUGC, K^{trans}, k_{ep}	—	No consistent relationship with clinical measures	Padhani et al. (44)
Recombinant human endostatin								
Mixed	rhEndostatin	10	Two-dimensional two slice	Measured	K^{trans}, v_e	Pixel based	No change in DCE-MRI biomarkers	Eder et al. (31)

(*Continued on the following page*)

Heterogeneity of Microvascular Structure

Human solid tumors are biologically heterogeneous (69), exhibiting considerable variation in microvascular structure and function (70, 71). In particular, growth factor expression is spatially heterogeneous within lesions of different size and may change during tumor growth (72). Furthermore, treatment of tumors with angiogenesis inhibitors has been shown to promote alternative angiogenic growth factor pathways, further promoting tumor heterogeneity (73). Imaging-based bio-markers have the potential to evaluate intratumoral heterogeneity and its relationship to tumor growth and response to therapy (2).

Technical considerations and practical approaches. The values of DCE-MRI variables are strongly affected by the definition of the tumor ROI. In each study, a decision must be made as to whether nonenhancing pixels are included in the ROI. Inclusion of zero values artificially lowers the mean and/or median variable values. Exclusion can obscure important heterogeneity information and can increase motion errors by effectively increasing the surface area of the normal tissue boundary around the sampled tumor. Three-dimensional ROI cover the entire tumor and are considered to be more accurate and reproducible than two-dimensional ROI, which are error prone despite attempts to correct for in-plane motion (36).

DCE-MRI data analysis assumes that signal intensity measurements taken over time originate from exactly the same volume of tissue in each sample. This is untrue outside of the brain due to physiologic (respiratory and cardiac) motion and patient movement. Use of a single ROI covering an entire tumor can reduce misregistration errors. Here, a single average enhancement curve can be extracted (34, 36, 37, 47, 51) to

Table 1. Selected trials of angiogenesis inhibitors evaluated by DCE-MRI (Cont'd)

Tumor group*	Agent	*n*	Acquisition	AIF[†]	DCE-MRI biomarker[‡]	ROI[§]	Principal findings	Reference
Anti-PDGFR-β antibody Fab′								
Mixed	CDP860	8	Three-dimensional	Measured	IAUGC, K^{trans}, v_e, v_p	Pixel based	No change in DCE-MRI biomarkers	Jayson et al. (32)
Anti-α_v integrin								
Mixed	CNTO 95	22	Three-dimensional	Measured	IAUGC, K^{trans}, v_e, v_p	Pixel based	Histogram showed difference in group K^{trans}	Watson et al. (89)
GBM	EMD 121974	21	T_2*-weighted	Measured	CBV, CBF	Pixel based	Reduction in gradient peak and enhancement	Akella et al. (27)
Flavonoid								
Mixed	DMXAA	16	Two-dimensional multislice	No model	SI metrics	Pixel based	Reduction in SI metrics	Galbraith et al. (54)
Antitubulin combretastatin analogue								
Mixed	CA-4-P	7	Two-dimensional single slice	No model	SI metrics	Whole tumor	Reduction in gradient peak and enhancement	Dowlatti et al. (51)
Mixed	CA-4-P	18	Two-dimensional multislice	Assumed (W)	IAUGC, K^{trans}, v_e	Pixel based	Dose-dependent reduction in K^{trans} defined dose	Galbraith et al. (53)
Mixed	CA-4-P	10	Three-dimensional	—	K^{trans}, v_e	Whole tumor	No consistent findings	Stevenson et al. (56)
Colchicine analogue								
Mixed	ZD6126	9	Three-dimensional	—	IAUGC	Pixel based	Dose-dependent reduction in IAUGC	Evelhoch et al. (52)

NOTE: Not all details were provided in some studies.

Abbreviations: GBM, glioblastoma multiforme; CRC, colorectal carcinoma; RCC, renal cell carcinoma; VEGF, vascular endothelial growth factor; PDGFR-β, platelet-derived growth factor receptor-β; FH, Fritz-Hansen method; W, Weinmann method; RR, response rate; PFS, progression-free survival; EES, extracellular extravascular space.

*Tumors were either mixed solid group, breast, glioblastoma multiforme, or colorectal or renal cell carcinoma.

[†]AIF was either measured or assumed by the Fritz-Hansen or Weinmann methods.

[‡]DCE-MRI biomarkers include (in table order) K^{trans} (volume transfer coefficient), k_{ep} (rate constant), v_p (blood plasma volume), v_e (volume of the EES), K_i (unidirectional influx), IAUGC (initial area under the gadolinium contrast agent concentration-time curve), CBV, CBF (cerebral blood flow), or SI (signal intensity) metrics.

[§]ROI analysis was either on a whole-tumor basis or pixel based.

[‖]All T_1-weighted acquisitions were at 1.5 T except Batchelor et al. (28), done at 3 T.

produce averaged kinetic variable estimates, for example of K^{trans}, for the entire tumor. However, this approach clearly ignores heterogeneity of tumor enhancement.

Alternatively, variables may be produced for each pixel (74), allowing the production of DCE-MRI variable maps, from which summary statistics, such as mean and/or median K^{trans}, may be calculated (28, 32, 33, 52, 53). This is routine practice in most cerebral studies because physiologic movement is negligible, allowing techniques such as tumor grading and targeted biopsy (19). However, the presence of motion reduces measurement reproducibility, especially in tumors with spatially heterogeneous enhancement around the edges of the selected ROI, resulting in a lower power to studies (75). Physiologic motion through the imaging plane further compounds motion error, particularly in studies that utilize a single imaging slice. Although these problems occur in whole-tumor ROI analysis, they are even greater in pixel mapping.

Hence, pixel mapping is technically challenging in areas of significant physiologic motion, such as the thorax and abdomen. Data may be acquired during breath holding (36, 56); however, such methods inevitably require concessions in the range and accuracy of biomarkers that can extracted (76). An alternative approach is to correct physiologic motion through postprocessing techniques (75). Spatial coregistration of MRI is routinely applied in dynamic brain imaging, but is more complex in the abdomen, where tissues are subject to greater motion and are not only displaced but also distorted during movement.

Specific DCE-MRI heterogeneity analysis techniques. Simple summary statistics (e.g., median K^{trans}) do not accurately describe heterogeneity within tumors (77). However, the distribution of variables can add further information. For example, the SD of pixel values for K^{trans} and similar variables within a ROI can improve diagnostic accuracy for distinguishing breast

cancer from benign lesions, compared with summary variables alone (78). In a study of high-grade gliomas, median K^{trans} did not relate to tumor grade or behavior, whereas measurement of the upper part of the distribution of K^{trans} (95th percentile) showed close correlation with overall survival (20). In another study, mean values of relative contrast agent recirculation—a variable that reflects areas of under perfusion—had no significant relationship with tumor behavior, although the distribution of pixel relative recirculation values followed a normal distribution in low-grade tumors but was significantly skewed toward higher values in glioblastoma multiforme (Fig. 3; ref. 79).

These alternative analysis techniques suggest that description of tumor heterogeneity is possible and that such analyses can significantly strengthen the use of DCE-MRI in studies of tumor pathophysiology or drug action, for example in detecting differential regional changes in the tumor core and enhancing rim (53). More specialized statistical analyses of heterogeneity based on DCE-MRI data are in their infancy but have already shown important clinical findings.

Data from several studies suggest that histogram analysis is sensitive at detecting change in tumor heterogeneity after treatment. In patients receiving cytotoxic chemotherapy for locally advanced breast cancer, SD and kurtosis of enhancement amplitude before therapy predicted subsequent radiological response. Furthermore, tumors that responded had significant reduction in SD of enhancement amplitude and showed change from a heterogeneous distribution into a more homogeneous one (80). Change in histogram heterogeneity has also been seen in a second clinical study of breast cancer (81) and in patients with rectal cancer after radiotherapy (82). Relative signal intensity (a model-free measure of tumor enhancement) of the 10th percentile has been shown to better predict tumor recurrence than mean or median relative signal intensity in patients with cervical carcinoma after radiotherapy

(83). Histograms of enhancement variables (including K^{trans}) have discriminated tumors treated with the thioredoxin-1 inhibitor PX-12 (Prolx Pharmaceuticals) versus untreated tumors in an animal model of colon cancer (84) and in a FSaII mouse fibrosarcoma models receiving NS-398 (85), where treated animals exhibited narrow homogeneously distributed histograms.

Interestingly, subtle or regional differences in antiangiogenic therapy efficacy can be shown using histogram analysis (Fig. 4), which may improve the overall sensitivity of preclinical studies and early-phase clinical trials. In one study, of the PC-3 prostate adenocarcinoma mouse tumor model, significant reductions in K^{trans} and the extracellular extravascular volume (v_e) were shown throughout entire tumors, after administration of the tyrosine kinase inhibitor ZD6474 (AstraZeneca). However, change in K^{trans} and v_e were significantly greater in the pixels corresponding to the lower 80% of absolute baseline K^{trans} values, which represented the tumor core (86). Importantly, application of a principal components analysis to the data showed disappearance of a second peak from a bimodal distribution after treatment—evidence of change in both the median value of K^{trans} and the heterogeneity within the tumor K^{trans} distribution (87). Tumor heterogeneity of response has also been shown in a mouse tumor model of human breast cancer after inhibition with AG-013736 (88). Histogram analysis of distributions of K^{trans} showed highly significant differences between progressive and stable disease in a phase I trial of the α_v-integrin receptor antibody (CNTO 95; Centocor; Fig. 5; ref. 89), although no significant changes were found in median K^{trans} in response to therapy (40).

Histogram analysis may be useful in grading tumors. In a limited number of studies, principally in gliomas, clear differences have been shown in both the median values of CBV and the distributions of values of normalized CBV for high-grade gliomas and cerebral metastases versus low-grade tumors (90).
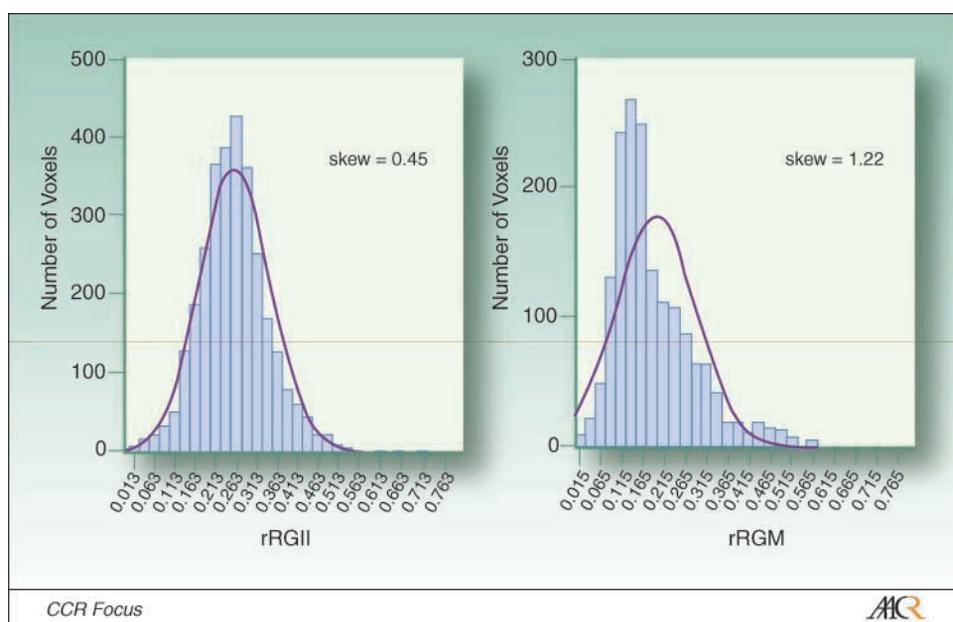

Fig. 3. Distribution of the values of relative recirculation (*rR*) in a low-grade (*left*) and high-grade (*right*) glioma. Note that the values are normally distributed in the low-grade tumor (with a skewness of 0.45) but show significant skew (1.22) toward the right of the distribution in the high-grade tumor.
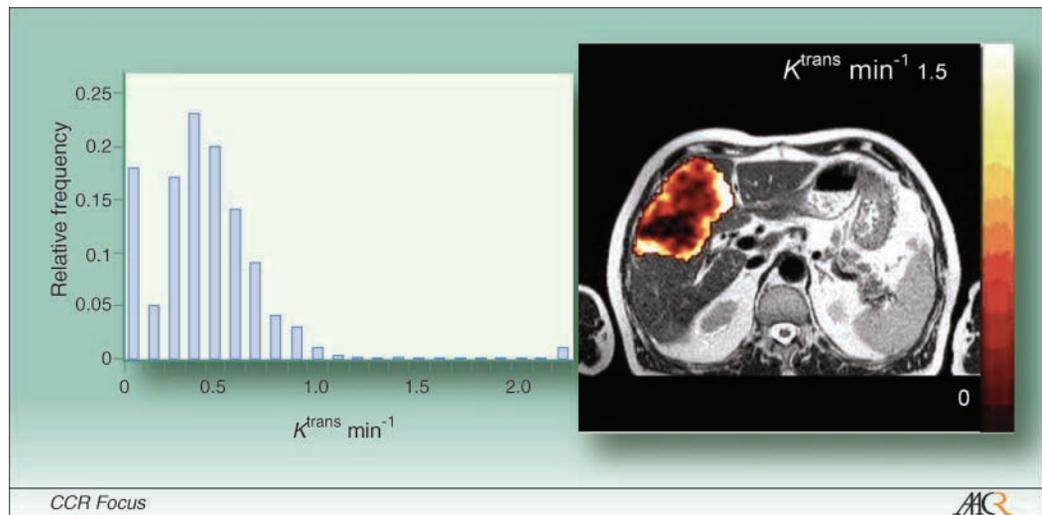
Fig. 4. Pixel map of K^{trans} within a liver metastasis from a primary colorectal cancer superimposed on a T_2-weighted anatomic image. It is clear that the distribution of pixel values of K^{trans} within the tumor is nonnormally distributed. Note that the pharmacokinetic model used has produced some (overestimated) nonphysiologic values of K^{trans}.

Furthermore, CBV pixel histogram analysis can accurately grade gliomas (91) and has been shown to detect and quantify subtle changes in tissue enhancement that predict disease progression (92). It is important to note that although histogram analysis may provide useful information regarding tumor heterogeneity, it does so at the expense of including spatial information.

Useful heterogeneity information may be produced from other features of the dynamic data series. One simple but powerful method is to measure the fraction of pixels that enhance after contrast agent administration. A phase I trial of CNTO 95 has shown that enhancing fraction can discriminate between stable and progressive disease in the absence of a clear treatment effect (40). More sophisticated approaches to assess spatial heterogeneity include fractal analysis, which

may provide useful markers of response to treatment (93). In another application of fractal analysis, v_e variable maps (a variable previously assumed to be of little physiologic interest) captured the heterogeneous nature of glioblastoma multiforme and predicted grade (94). Finally, factor analysis enables the characterization of the signal intensity profiles within a tumor and can identify intratumoral heterogeneity, as shown by facilitating prediction of response to chemotherapy in patients with osteosarcoma (22).

Conclusion

DCE-MRI has been shown to provide noninvasive imaging biomarkers of tumor biological response to antiangiogenic and

Fig. 5. Histograms of K^{trans} distribution in a study of the antiangiogenic agent CNTO 95 in mixed solid tumors. Data are subdivided into those showing stable or better disease at follow-up versus those with disease progression. Although no significant difference was found in median K^{trans} between these groups, significant differences were seen in histogram analysis (adapted with permission from ISMRM from ref. 89).
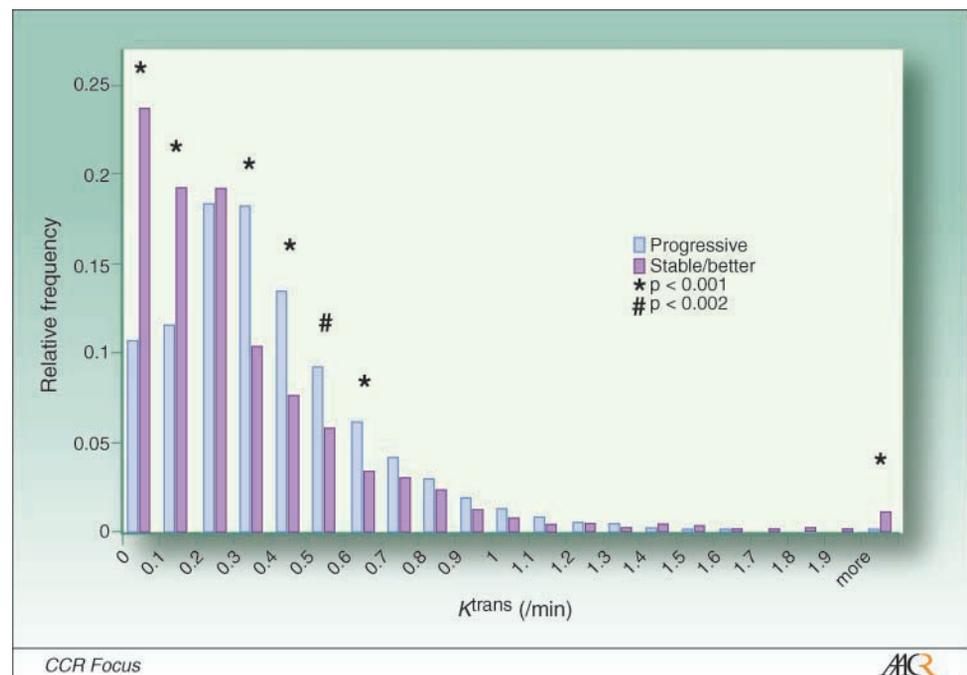
vascular targeting agents in a number of clinical trials. It also has an increasing number of clinical applications. Although further animal and clinical validation of analytic techniques are required, DCE-MRI appears to be a useful tool in the investigation of tumor heterogeneity and has already shown its potential to improve sensitivity to subtle drug effects and provide additional understanding of tumor biology and response to therapy.

Appendix. Magnetic Resonance Imaging Techniques

Image acquisition strategies. Principal contrast mechanisms in MRI emerge from the relaxation properties of tissue water (or fat) hydrogen nuclei in the scanner magnetic field after undergoing radiofrequency excitation. These properties can be manipulated to reflect features of the molecular and physiologic environment of a tissue. T_1-weighted images emphasize the rate (different for different tissue types) at which energy is redistributed between these nuclei and the tissue as a whole. T_2^*-weighted images emphasize the different rates at which the same nuclei lose phase coherence with one another and the way that this process is affected by local variations in field strength due to differences in magnetic susceptibility between tissues. Conventional gadolinium chelate-based contrast media affect T_1-weighted images causing a signal increase, and T_2^*-weighted images causing a signal decrease.

Nearly all clinical DCE-MRI is done at 1.5 T. The data have a typical spatial resolution of a few millimeters, which reflects the technical limits of the scanner specifications and the need for an acceptable signal-to-noise ratio. This, in turn, limits temporal resolution, in-plane resolution, and the number of slices that can be imaged. There is a direct trade-off between these factors so that rapid sampling at high spatial resolution can be achieved only by sacrificing the volume of tumor sampled (6, 95).

Dynamic susceptibility contrast MRI. T_2^* dynamic imaging acquisitions have been widely used in the brain (96), where rapid loss of magnetic resonance signal is used to calculate the change in concentration of contrast agent for each individual voxel. Studies typically use fast imaging techniques such as single or multishot echo planar imaging to produce a temporal resolution of around 2 s, during which it is possible to acquire 5 to 15 slices at a matrix resolution of 128×128 or greater, depending on scanner specifications. The acquisition variables vary hugely in T_2 and T_2^* dynamic imaging but all have a long time to repetition (e.g., 200-2,000 ms) and a long echo time (e.g., 50 ms; ref. 95).

Analysis of T_2^*-weighted DCE-MRI is mainly relevant to a small number of glioma studies and the reader should refer to references (97, 98) for a more detailed description. In brief, the high initial concentration of contrast agent during the first pass makes T_2- and T_2^*-weighted imaging sensitive to both flow and blood volume; hence, measures of the CBV and cerebral blood flow are commonly done (95). It is important to note that the contrast agent is assumed to remain in the vessels as a blood pool marker throughout the examination (99, 100). This is untrue in malignancy, where leakage of contrast agent occurs through a disrupted blood-brain barrier. Also, T_2^* techniques generally suffer from susceptibility artifacts at interfaces between air and fat/soft tissue, further limiting their use outside the brain.

T_1-weighted DCE-MRI: data acquisition and analysis. Most DCE-MRI studies use T_1-weighted images, which are generally less sensitive to susceptibility artifact and allow estimation of capillary permeability and surface area. Investigators usually adopt a single/multislice or three-dimensional gradient echo sequence. Typical scan variables include a time to repetition of 3 to 10 ms, echo time under 5 ms, a variety of choice of flip angle, and in-plane imaging matrix between 128×128 and 256×256 at a spatial resolution of a few millimeters (32, 36, 44). Volumetric acquisition methods allow up to around 25 slices to be acquired over a period in excess of 5 min to provide adequate data. Pharmacokinetic analysis of contrast agent distribution requires transformation of measurements of signal change over time to measurements of contrast agent concentration (5). For T_1-weighted protocols, the relationship between signal change and contrast concentration is nonlinear; thus, a separate measurement of baseline T_1 values is done before the dynamic series (101, 102).

Pharmacokinetic analyses are complex and the choice of technique has major effect on the meaning of the derived variables. The IAUGC (103) is the simplest pharmacokinetic variable and appears reproducible. This is simply a measure of the amount of contrast agent delivered to and retained in the tumor tissue over a given time period and offers no biological specificity (2, 5). All other pharmacokinetic analyses use curve fitting to characterize the tissue contrast agent concentration curve, together with an estimate of the AIF, which needs to be measured in each patient (104) to portray the ''true'' input function for each tumor (5). However, accurate measurement of the AIF is technically demanding, due to blood flow artifacts in the image (101, 105), and requires high temporal resolution of less than a second (106). Such rapid data acquisition considerably limits the spatial resolution and extent of tissue coverage that can be achieved. An alternative approach adopts an idealized AIF—generally from population-based studies of contrast agent clearance from the blood pool—which relaxes requirements on temporal resolution, slice positioning, and sequence choice (107, 108).

Modeled variables are in theory independent of the scanning acquisition protocol, thus avoiding problems associated with signal intensity metrics, supporting their use in multicenter studies (26, 33). Simple analyses based on the Kety model provide estimates of K^{trans} (or a related variable, K_i) and v_e (109, 110). Here, changes in K^{trans} reflect changes in blood flow, blood volume, endothelial permeability and endothelial surface area and the individual effects of each component cannot be distinguished (5). These models are widely used but assume that signal change results entirely from contrast agent in the extravascular space. This produces significant errors in voxels that contain large vascular spaces—a relatively common occurrence in tumors (74, 111).

Attempts have been made to provide more accurate estimates of individual microvascular variables, particularly the signal contribution produced by contrast medium within blood plasma volume (112), and to model perfusion (F) and the product of capillary endothelial permeability and capillary surface area (113). These more complex models appear

Table 2. List of abbreviations and standard terms commonly used in DCE-MRI pharmacokinetic analyses

Symbol	Short name	Unit	End point
K^{trans}	Volume transfer constant between plasma and EES	min^{-1}	Primary
k_{ep}	Rate constant between EES and plasma	min^{-1}	Secondary
K_i	Unidirectional transfer constant	min^{-1}	—
C_p	Tracer concentration in arterial blood plasma	mmol/L	—
$C(t)$	Concentration of contrast agent at time t in each voxel	mmol/L	—
v_e	Volume of EES per unit volume tissue	None	Secondary
v_p	Blood plasma volume	None	Secondary
CBV	Cerebral blood volume	mL	Primary
E	Initial extraction ratio	—	—
F	Flow	$mL\ g^{-1}\ min^{-1}$	—
P	Total capillary wall permeability	$cm\ min^{-1}$	—
PS	Permeability-surface area product per unit mass of tissue	$mL\ min^{-1}$	—
IAUGC	Initial area under gadolinium concentration agent- time curve	mmol/L Gd min	Primary

NOTE: Data were adapted from ref. 4.
Abbreviation: EES, extracellular extravascular space.

desirable because they allow specific analysis of biological effects; however, increasing the number of variables involved in the curve fitting process produces concomitant reductions in accuracy and reproducibility (9, 62). Therefore, many investigators calculate the IAUGC, which partially reflects K^{trans}, v_e, and v_p (114), and choose one or more of the modeled variables; choice of pharmacokinetic model depends on the degree of specificity required with regard to the mechanism of drug action, the acceptable level of reproducibility in the estimation of biomarkers, and the quality of acquired MRI data. Commonly used variables in DCE-MRI studies (4) are summarized in Table 2.

Acknowledgments

References

1. Jackson A, Buckley DL, Parker GJM. Dynamic contrast-enhanced magnetic resonance imaging in oncology. Berlin: Springer; 2005.
2. Leach MO, Brindle KM, Evelhoch JL, et al. The assessment of antiangiogenic and antivascular therapies in early-stage clinical trials using magnetic resonance imaging: issues and recommendations. Br J Cancer 2005;92:1599–610.
3. Blasberg R. Imaging update: new windows, new views. Clin Cancer Res 2007;13:3444–8.
4. Tofts PS, Brix G, Buckley DL, et al. Estimating kinetic parameters from dynamic contrast-enhanced T(1)-weighted MRI of a diffusable tracer: standardized quantities and symbols. J Magn Reson Imaging 1999;10:223–32.
5. Parker GJM, Buckley DL. Tracer Kinetic Modelling for T₁-weighted DCE-MRI. In: Jackson A, Buckley DL, Parker GJM, editors. Dynamic contrast-enhanced magnetic resonance imaging in oncology. Berlin: Springer 2005; p. 81–92.
6. Buckley DL, Parker GJM. Measuring contrast agent concentration in T₁-weighted dynamic contrast-enhanced MRI. In: Jackson A, Buckley DL, Parker GJM, editors. Dynamic contrast-enhanced magnetic resonance imaging in oncology. Berlin: Springer-Verlag 2005; p.69–79.
7. Stack J, Redmond O, Codd M, et al. Breast disease: tissue characterization with Gd-DTPA enhancement profiles. Radiology 1990;174:491–4.
8. Flickinger F, Allison J, Sherry R, Wright J. Differentiation of benign from malignant breast masses by time-intensity evaluation of contrast enhanced MRI. Magn Reson Imaging 1993;11:617–20.
9. Roberts C, Issa B, Stone A, et al. Comparative study into the robustness of compartmental modeling and model-free analysis in DCE-MRI studies. J Magn Reson Imaging 2006;23:554–63.

10. Knopp MV, Weiss E, Sinn HP, et al. Pathophysiologic basis of contrast enhancement in breast tumors. J Magn Reson Imaging 1999;10:260–6.
11. Kuhl CK, Mielcareck P, Klaschik S, et al. Dynamic breast MR imaging: are signal intensity time course data useful for differential diagnosis of enhancing lesions? Radiology 1999;211:101–10.
12. Goto M, Ito H, Akazawa K, et al. Diagnosis of breast tumors by contrast-enhanced MR imaging: comparison between the diagnostic performance of dynamic enhancement patterns and morphologic features. J Magn Reson Imaging 2007;25:104–12.
13. Narisada H, Aoki T, Sasaguri T, et al. Correlation between numeric gadolinium-enhanced dynamic MRI ratios and prognostic factors and histologic type of breast carcinoma. AJR Am J Roentgenol 2006;187:297–306.
14. Takeda Y, Yoshikawa K. Contrast-enhanced dynamic MR imaging parameters and histological types of invasive ductal carcinoma of breast. Biomed Pharmacother 2005;59:115–21.
15. Jackson A, Haroon H, Zhu XP, et al. Breath-hold perfusion and permeability mapping of hepatic malignancies using magnetic resonance imaging and a first-pass leakage profile model. NMR Biomed 2002;15:164–73.
16. Aronen HJ, Glass J, Pardo FS, et al. Echo-planar MR cerebral blood volume mapping of gliomas. Clinical utility. Acta Radiol 1995;36:520–8.
17. Aronen HJ, Pardo FS, Kennedy DN, et al. High microvascular blood volume is associated with high glucose uptake and tumor angiogenesis in human gliomas. Clin Cancer Res 2000;6:2189–200.
18. Patankar TF, Haroon HA, Mills SJ, et al. Is volume transfer coefficient (Ktrans) related to histologic grade in human gliomas? AJNR Am J Neuroradiol 2005;26:2455–65.

19. Knopp EA, Cha S, Johnson G, et al. Glial neoplasms: dynamic contrast-enhanced T₂*-weighted MR imaging. Radiology 1999;211:791–8.
20. Mills SJ, Patankar TA, Haroon HA, et al. Do cerebral blood volume and contrast transfer coefficient predict prognosis in human glioma? AJNR Am J Neuroradiol 2006;27:853–8.
21. Buckley DL, Roberts C, Parker GJ, Logue JP, Hutchinson CE. Prostate cancer: evaluation of vascular characteristics with dynamic contrast-enhanced T₁-weighted MR imaging-initial experience. Radiology 2004;233:709–15.
22. Bonnerot V, Charpentier A, Frouin F, et al. Factor analysis of dynamic magnetic resonance imaging in predicting the response of osteosarcoma to chemotherapy. Invest Radiol 1992;27:847–55.
23. Mayr NA, Yuh WT, Magnotta VA, et al. Tumor perfusion studies using fast magnetic resonance imaging technique in advanced cervical cancer: a new noninvasive predictive assay. Int J Radiat Oncol Biol Phys 1996;36:623–33.
24. Hillengass J, Wasser K, Delorme S, et al. Lumbar bone marrow microcirculation measurements from dynamic contrast-enhanced magnetic resonance imaging is a predictor of event-free survival in progressive multiple myeloma. Clin Cancer Res 2007;13:475–81.
25. Zahra MA, Hollingsworth KG, Sala E, Lomas DJ, Tan LT. Dynamic contrast-enhanced MRI as a predictor of tumour response to radiotherapy. Lancet Oncol 2007;8:63–74.
26. Padhani AR, Husband JE. Dynamic contrast-enhanced MRI studies in oncology with an emphasis on quantification, validation and human studies. Clin Radiol 2001;56:607–20.
27. Akella NS, Twieg DB, Mikkelsen T, et al. Assessment of brain tumor angiogenesis inhibitors using perfusion magnetic resonance imaging: quality and analysis

results of a phase I trial. J Magn Reson Imaging 2004; 20:913–22.

28. Batchelor TT, Sorensen AG, di Tomaso E, et al. AZD2171, a pan-VEGF receptor tyrosine kinase inhibitor, normalizes tumor vasculature and alleviates edema in glioblastoma patients. Cancer Cell 2007;11:83–95.

29. Conrad C, Friedman H, Reardon D, et al. A phase I/II trial of single-agent PTK 787/ZK 222584 (PTK/ZK), a novel, oral angiogenesis inhibitor, in patients with recurrent glioblastoma multiforme (GBM). J Clin Oncol (Meet Abstr) 2004;22:1512.

30. Drevs J, Medinger M, Mross K, et al. Phase I clinical evaluation of AZD2171, a highly potent VEGF receptor tyrosine kinase inhibitor, in patients with advanced tumors. J Clin Oncol (Meet Abstr) 2005;23:3002.

31. Eder JP, Jr., Supko JG, Clark JW, et al. Phase I clinical trial of recombinant human endostatin administered as a short intravenous infusion repeated daily. J Clin Oncol 2002;20:3772–84.

32. Jayson GC, Parker GJ, Mullamitha S, et al. Blockade of platelet-derived growth factor receptor-β by CDP860, a humanized, PEGylated di-Fab′, leads to fluid accumulation and is associated with increased tumor vascularized volume. J Clin Oncol 2005;23: 973–81.

33. Jayson GC, Zweit J, Jackson A, et al. Molecular imaging and biological evaluation of HuMV833 anti-VEGF antibody: implications for trial design of antiangiogenic antibodies. J Natl Cancer Inst 2002;94: 1484–93.

34. Liu G, Rugo HS, Wilding G, et al. Dynamic contrast-enhanced magnetic resonance imaging as a pharmacodynamic measure of response after acute dosing of AG-013736, an oral angiogenesis inhibitor, in patients with advanced solid tumors: results from a phase I study. J Clin Oncol 2005;23:5464–73.

35. Medved M, Karczmar G, Yang C, et al. Semiquantitative analysis of dynamic contrast enhanced MRI in cancer patients: variability and changes in tumor tissue over time. J Magn Reson Imaging 2004;20: 122–8.

36. Morgan B, Thomas AL, Drevs J, et al. Dynamic contrast-enhanced magnetic resonance imaging as a biomarker for the pharmacological response of PTK787/ZK 222584, an inhibitor of the vascular endothelial growth factor receptor tyrosine kinases, in patients with advanced colorectal cancer and liver metastases: results from two phase I studies. J Clin Oncol 2003;21:3955–64.

37. Mross K, Drevs J, Muller M, et al. Phase I clinical and pharmacokinetic study of PTK/ZK, a multiple VEGF receptor inhibitor, in patients with liver metastases from solid tumours. Eur J Cancer 2005;41:1291–9.

38. Mross K, Scheulen M, Frost A, et al. Phase I study of BAY 57-9352, a VEGFR-2 inhibitor, in cycles of 14 days on/7 days off in patients with advanced solid tumors. J Clin Oncol (Meet Abstr) 2006;24:3089.

39. Mross KB, Gmehling D, Frost A, et al. A clinical Phase I, pharmacokinetic (PK), and pharmacodynamic study of twice daily BIBF 1120 in advanced cancer patients. J Clin Oncol (Meet Abstr) 2005;23:3031.

40. Mullamitha SA, Ton NC, Parker GJ, et al. Phase I evaluation of a fully human anti-{α}v integrin monoclonal antibody (CNTO 95) in patients with advanced solid tumors. Clin Cancer Res 2007;13:2128–35.

41. O'Donnell A, Padhani A, Hayes C, et al. A Phase I study of the angiogenesis inhibitor SU5416 (semaxanib) in solid tumours, incorporating dynamic contrast MR pharmacodynamic end points. Br J Cancer 2005; 93:876–83.

42. O'Dwyer PJ, Rosen M, Gallagher M, Schwartz B, Flaherty KT. Pharmacodynamic study of BAY 43–9006 in patients with metastatic renal cell carcinoma. J Clin Oncol (Meet Abstr) 2005;23:3005.

43. Overmoyer B, Silverman P, Leeming R, et al. Phase II trial of neoadjuvant docetaxel with or without bevacizumab in patients with locally advanced breast cancer. J Clin Oncol 2004;22:727.

44. Padhani AR, Taylor NJ, d'Arcy JA, et al. Dynamic MRI evaluation of the triple receptor tyrosine kinase inhibitor BIBF 1120 in patients with advanced solid tumours. Proc Intl Soc Magn Reson Med 2006;14:765.

45. Rosen LS, Kurzrock R, Jackson E, et al. Safety and pharmacokinetics of AMG 706 in patients with advanced solid tumors. J Clin Oncol (Meet Abstr) 2005;23:3013.

46. Rosen LS, Wilding G, Sweeney C, et al. Phase I dose escalation study to determine the safety, pharmacokinetics and pharmacodynamics of BMS-582664, a VEGFR/FGFR inhibitor in patients with advanced/metastatic solid tumors. J Clin Oncol (Meet Abstr) 2006;24:3051.

47. Thomas AL, Morgan B, Horsfield MA, et al. Phase I study of the safety, tolerability, pharmacokinetics, and pharmacodynamics of PTK787/ZK 222584 administered twice daily in patients with advanced cancer. J Clin Oncol 2005;23:4162–71.

48. Thomas JP, Arzoomanian RZ, Alberti D, et al. Phase I pharmacokinetic and pharmacodynamic study of recombinant human endostatin in patients with advanced solid tumors. J Clin Oncol 2003;21:223–31.

49. Wedam SB, Low JA, Yang SX, et al. Antiangiogenic and antitumor effects of bevacizumab in patients with inflammatory and locally advanced breast cancer. J Clin Oncol 2006;24:769–77.

50. Xiong HQ, Herbst R, Faria SC, et al. A phase I surrogate endpoint study of SU6668 in patients with solid tumors. Invest New Drugs 2004;22:459–66.

51. Dowlati A, Robertson K, Cooney M, et al. A phase I pharmacokinetic and translational study of the novel vascular targeting agent combretastatin a-4 phosphate on a single-dose intravenous schedule in patients with advanced cancer. Cancer Res 2002;62: 3408–16.

52. Evelhoch JL, LoRusso PM, He Z, et al. Magnetic resonance imaging measurements of the response of murine and human tumors to the vascular-targeting agent ZD6126. Clin Cancer Res 2004;10:3650–7.

53. Galbraith SM, Maxwell RJ, Lodge MA, et al. Combretastatin A4 phosphate has tumor antivascular activity in rat and man as demonstrated by dynamic magnetic resonance imaging. J Clin Oncol 2003;21: 2831–42.

54. Galbraith SM, Rustin GJ, Lodge MA, et al. Effects of 5,6-dimethylxanthenone-4-acetic acid on human tumor microcirculation assessed by dynamic contrast-enhanced magnetic resonance imaging. J Clin Oncol 2002;20:3826–40.

55. McKeage MJ, Fong P, Jeffery M, et al. 5,6-Dimethylxanthenone-4-acetic acid in the treatment of refractory tumors: a phase I safety study of a vascular disrupting agent. Clin Cancer Res 2006;12:1776–84.

56. Stevenson JP, Rosen M, Sun W, et al. Phase I trial of the antivascular agent combretastatin A4 phosphate on a 5-day schedule to patients with cancer: magnetic resonance imaging evidence for altered tumor blood flow. J Clin Oncol 2003;21:4428–38.

57. O'Connor JP, Jackson A, Parker GJ, Jayson GC. DCE-MRI biomarkers in the clinical evaluation of antiangiogenic and vascular disrupting agents. Br J Cancer 2007;96:189–95.

58. Galbraith SM, Lodge MA, Taylor NJ, et al. Reproducibility of dynamic contrast-enhanced MRI in human muscle and tumours: comparison of quantitative and semi-quantitative analysis. NMR Biomed 2002; 15:132–42.

59. Padhani AR, Hayes C, Landau S, Leach MO. Reproducibility of quantitative dynamic MRI of normal human tissues. NMR Biomed 2002;15:143–53.

60. Thomas AL, Morgan B, Drevs J, et al. Vascular endothelial growth factor receptor tyrosine kinase inhibitors: PTK787/ZK 222584. Semin Oncol 2003;30: 32–8.

61. Hecht J, Trarbach T, Jaeger E, et al. A randomized, double-blind, placebo-controlled, phase III study in patients (Pts) with metastatic adenocarcinoma of the colon or rectum receiving first-line chemotherapy with oxaliplatin/5-fluorouracil/leucovorin and PTK787/ZK 222584 or placebo (CONFIRM-1). J Clin Oncol (Meet Abstr) 2005;23:3.

62. Buckley DL. Uncertainty in the analysis of tracer kinetics using dynamic contrast-enhanced T1-weighted MRI. Magn Reson Med 2002;47:601–6.

63. Jayson GC, Waterton JC. Applications of dynamic contrast-enhanced MRI in oncology drug development. In: Jackson A, Buckley DL, Parker GJM, editors. Dynamic contrast-enhanced magnetic resonance imaging in oncology. Berlin: Springer 2005; p. 281–97.

64. Buckley DL, Drew PJ, Mussurakis S, Monson JR, Horsman A. Microvessel density of invasive breast cancer assessed by dynamic Gd-DTPA enhanced MRI. J Magn Reson Imaging 1997;7:461–4.

65. Stomper PC, Winston JS, Herman S, et al. Angiogenesis and dynamic MR imaging gadolinium enhancement of malignant and benign breast lesions. Breast Cancer Res Treat 1997;45:39–46.

66. Hulka CA, Edmister WB, Smith BL, et al. Dynamic echo-planar imaging of the breast: experience in diagnosing breast carcinoma and correlation with tumor angiogenesis. Radiology 1997;205:837–42.

67. Mayr NA, Yuh WT, Zheng J, et al. Prediction of tumor control in patients with cervical cancer: analysis of combined volume and dynamic enhancement pattern by MR imaging. AJR Am J Roentgenol 1998;170: 177–82.

68. Hawighorst H, Knapstein PG, Knopp MV, et al. Uterine cervical carcinoma: comparison of standard and pharmacokinetic analysis of time-intensity curves for assessment of tumor angiogenesis and patient survival. Cancer Res 1998;58:3598–602.

69. Heppner GH. Tumor heterogeneity. Cancer Res 1984;44:2259–65.

70. Carmeliet P, Jain RK. Angiogenesis in cancer and other diseases. Nature 2000;407:249–57.

71. Gillies RJ, Schornack PA, Secomb TW, Raghunand N. Causes and effects of heterogeneous perfusion in tumors. Neoplasia 1999;1:197–207.

72. Kumar R, Kuniyasu H, Bucana CD, Wilson MR, Fidler IJ. Spatial and temporal expression of angiogenic molecules during tumor growth and progression. Oncol Res 1998;10:301–11.

73. Casanovas O, Hicklin DJ, Bergers G, Hanahan D. Drug resistance by evasion of antiangiogenic targeting of VEGF signaling in late-stage pancreatic islet tumors. Cancer Cell 2005;8:299–309.

74. Parker GJ, Suckling J, Tanner SF, et al. Probing tumor microvascularity by measurement, analysis and display of contrast agent uptake kinetics. J Magn Reson Imaging 1997;7:564–74.

75. Buonaccorsi GA, Roberts C, Cheung S, et al. Comparison of the performance of tracer kinetic model-driven registration for dynamic contrast enhanced MRI using different models of contrast enhancement. Acad Radiol 2006;13:1112–23.

76. Li KL, Jackson A. New hybrid technique for accurate and reproducible quantitation of dynamic contrast-enhanced MRI data. Magn Reson Med 2003;50: 1286–95.

77. Walker-Samuel S, Taylor NJ, Padhani AR, Leach MO, Collins DJ. The effect of heterogeneous tumour enhancement on the assessment of response to treatment. Proc Intl Soc Magn Reson Med 2006;14:761.

78. Issa B, Buckley DL, Turnbull LW. Heterogeneity analysis of Gd-DTPA uptake: improvement in breast lesion differentiation. J Comput Assist Tomogr 1999; 23:615–21.

79. Jackson A, Kassner A, Annesley-Williams D, et al. Abnormalities in the recirculation phase of contrast agent bolus passage in cerebral gliomas: comparison with relative blood volume and tumor grade. AJNR Am J Neuroradiol 2002;23:7–14.

80. Chang YC, Huang CS, Liu YJ, et al. Angiogenic response of locally advanced breast cancer to neoadjuvant chemotherapy evaluated with parametric

histogram from dynamic contrast-enhanced MRI. Phys Med Biol 2004;49:3593–602.

81. Hayes C, Padhani AR, Leach MO. Assessing changes in tumour vascular function using dynamic contrast-enhanced magnetic resonance imaging. NMR Biomed 2002;15:154–63.

82. de Lussanet QG, Backes WH, Griffioen AW, et al. Dynamic contrast-enhanced magnetic resonance imaging of radiation therapy-induced microcirculation changes in rectal cancer. Int J Radiat Oncol Biol Phys 2005;63:1309–15.

83. Mayr NA, Yuh WT, Arnholt JC, et al. Pixel analysis of MR perfusion imaging in predicting radiation therapy outcome in cervical cancer. J Magn Reson Imaging 2000;12:1027–33.

84. Jordan BF, Runquist M, Raghunand N, et al. The thioredoxin-1 inhibitor 1-methylpropyl 2-imidazolyl disulfide (PX-12) decreases vascular permeability in tumor xenografts monitored by dynamic contrast enhanced magnetic resonance imaging. Clin Cancer Res 2005;11:529–36.

85. Crokart N, Radermacher K, Jordan BF, et al. Tumor radiosensitization by antiinflammatory drugs: evidence for a new mechanism involving the oxygen effect. Cancer Res 2005;65:7911–6.

86. Checkley D, Tessier JJ, Kendrew J, Waterton JC, Wedge SR. Use of dynamic contrast-enhanced MRI to evaluate acute treatment with ZD6474, a VEGF signalling inhibitor, in PC-3 prostate tumours. Br J Cancer 2003;89:1889–95.

87. O'Connor EL, Fieller N, Holmes A, Waterton J. How to analyse dynamic MRI in oncology; advanced histogram analysis gives better statistical power & insight than simple averaging. Proc Intl Soc Magn Reson Med 2005;13:2101.

88. Li KL, Wilmes LJ, Henry RG, et al. Heterogeneity in the angiogenic response of a BT474 human breast cancer to a novel vascular endothelial growth factor-receptor tyrosine kinase inhibitor: assessment by voxel analysis of dynamic contrast-enhanced MRI. J Magn Reson Imaging 2005;22:511–9.

89. Watson Y, Cheung S, Roberts C, et al. Prognostic power of DCE-MRI heterogeneity analysis in patients with advanced solid tumors. Proc Intl Soc Magn Reson Med 2006;14:755.

90. Emblem KE, Nedregaard B, Due-Tonnessen P, et al. Characterization of intra-axial neoplasms by histogram analysis of total tumor volume from MR-derived cerebral blood volume maps. Proc Int Soc Magn Reson Med 2006;14:823.

91. Young RJ, Pollack E, Lu H, et al. Region-of-interest analysis vs. non-region-of-interest histogram analysis in the evaluation of cerebral gliomas. Proc Int Soc Magn Reson Med 2006;14:3158.

92. Tofts PS, Benton CE, Weil RS, et al. Quantitative analysis of whole-tumor Gd enhancement histograms predicts malignant transformation in low-grade gliomas. J Magn Reson Imaging 2007;25:208–14.

93. Dzik-Jurasz A, Walker-Samuel S, Leach MO, et al. Fractal parameters derived from analysis of DCE-MRI data correlates with response to therapy in rectal carcinoma. Proc Int Soc Magn Reson Med 2004;2:2503.

94. Rose CJ, Buonaccorsi GA, Cheung S, et al. Fractal properties of tumours in dynamic contrast enhanced magnetic resonance imaging. Proc Int Soc Reson Med. 2007;15:2821.

95. Jackson A. Analysis of dynamic contrast enhanced MRI. Br J Radiol 2004;77 Spec No 2:S154–66.

96. Barbier EL, Lamalle L, Decorps M. Methodology of brain perfusion imaging. J Magn Reson Imaging 2001; 13:496–520.

97. Weisskoff R, Boxerman J, Sorensen A, et al. Simultaneous blood volume and permeability mapping using a single Gd-based contrast injection. Proc Int Soc Magn Reson Med 1994;2:279.

98. Kassner A, Annesley DJ, Zhu XP, et al. Abnormalities of the contrast re-circulation phase in cerebral tumors demonstrated using dynamic susceptibility contrast-enhanced imaging: a possible marker of vascular tortuosity. J Magn Reson Imaging 2000;11:103–13.

99. Rosen BR, Belliveau JW, Aronen HJ, et al. Susceptibility contrast imaging of cerebral blood volume: human experience. Magn Reson Med 1991;22:293–9.

100. Ostergaard L, Johannsen P, Host Poulsen P, et al. Cerebral blood flow measurements by magnetic resonance imaging bolus tracking: comparison with [O15] H_2O positron emission tomography in humans. J Cereb Blood Flow Metab 1998;18:935–40.

101. Zhu XP, Li KL, Kamaly-Asl ID, et al. Quantification of endothelial permeability, leakage space, and blood volume in brain tumors using combined T_1 and T_2* contrast-enhanced dynamic MR imaging. J Magn Reson Imaging 2000;11:575–85.

102. Haase A. Snapshot FLASH MRI. Applications to T_1, T_2, and chemical-shift imaging. Magn Reson Med 1990;13:77–89.

103. Evelhoch JL. Key factors in the acquisition of contrast kinetic data for oncology. J Magn Reson Imaging 1999;10:254–9.

104. Parker GJ, Roberts C, Macdonald A, et al. Experimentally-derived functional form for a population-averaged high-temporal-resolution arterial input function for dynamic contrast-enhanced MRI. Magn Reson Med 2006;56:993–1000.

105. Li K, Zhu X, Waterton J, Jackson A. Improved 3D quantitative mapping of blood volume and endothelial permeability in brain tumours. J Magn Reson Imaging 2000;12:347–57.

106. Henderson E, Rutt BK, Lee TY. Temporal sampling requirements for the tracer kinetics modeling of breast disease. Magn Reson Imaging 1998;16:1057–73.

107. Weinmann HJ, Laniado M, Mutzel W. Pharmacokinetics of GdDTPA/dimeglumine after intravenous injection into healthy volunteers. Physiol Chem Phys Med NMR 1984;16:167–72.

108. Fritz-Hansen T, Rostrup E, Larsson HB, et al. Measurement of the arterial concentration of Gd-DTPA using MRI: a step toward quantitative perfusion imaging. Magn Reson Med 1996;36:225–31.

109. Tofts PS, Kermode AG. Measurement of the blood brain barrier permeability and leakage space using dynamic MR imaging: fundamental concepts. Magn Reson Med 1991;17:357–67.

110. Larsson HB, Stubgaard M, Frederiksen JL, et al. Quantitation of blood-brain barrier defect by magnetic resonance imaging and gadolinium-DTPA in patients with multiple sclerosis and brain tumors. Magn Reson Med 1990;16:117–31.

111. Haroon HA, Buckley DL, Patankar TA, et al. A comparison of K_{trans} measurements obtained with conventional and first pass pharmacokinetic models in human gliomas. J Magn Reson Imaging 2004;19:527–36.

112. Tofts PS. Modeling tracer kinetics in dynamic Gd-DTPA MR imaging. J Magn Reson Imaging 1997;7:91–101.

113. St Lawrence K, Lee T. An Adiabatic Approximation to the tissue homogeneity model for water exchange in the brain: i. theoretical derivation. J Cereb Blood Flow Metab 1998;18:1365–77.

114. Walker-Samuel S, Leach MO, Collins DJ. Evaluation of response to treatment using DCE-MRI: the relationship between initial area under the gadolinium curve (IAUGC) and quantitative pharmacokinetic analysis. Phys Med Biol 2006;51:3593–602.

Imaging Tumor Vascular Heterogeneity and Angiogenesis using Dynamic Contrast-Enhanced Magnetic Resonance Imaging

Alan Jackson, James P.B. O'Connor, Geoff J.M. Parker, et al.

Updated version	Access the most recent version of this article at: http://clincancerres.aacrjournals.org/content/13/12/3449

Cited articles	This article cites 110 articles, 25 of which you can access for free at: http://clincancerres.aacrjournals.org/content/13/12/3449.full#ref-list-1
Citing articles	This article has been cited by 27 HighWire-hosted articles. Access the articles at: http://clincancerres.aacrjournals.org/content/13/12/3449.full#related-urls

E-mail alerts	Sign up to receive free email-alerts related to this article or journal.
Reprints and Subscriptions	To order reprints of this article or to subscribe to the journal, contact the AACR Publications Department at pubs@aacr.org.
Permissions	To request permission to re-use all or part of this article, use this link http://clincancerres.aacrjournals.org/content/13/12/3449. Click on "Request Permissions" which will take you to the Copyright Clearance Center's (CCC) Rightslink site.